CLASSICAL MODEL OF THE ELECTROMAGNETIC INTERACTION SUITABLE FOR HIGH SPEED SEMICONDUCTOR DEVICE SIMULATION

Matt Grupen
High Performance Technologies, Inc.
US Army Research Lab
Aberdeen Proving Ground, MD 21005

ABSTRACT

The vector field relations and mobile charge thermodynamics that form a complete and self-consistent classical model of the electromagnetic interaction are presented. The charge thermodynamics includes an original treatment of heat flow between ideal Fermi gases that is derived from their heat capacities. An original discretization scheme based on the properties of Delaunay and Voronoi meshes is also presented. This new scheme allows the field equations to be solved self-consistently with the highly nonlinear charge transport equations, producing the fully coupled dynamics of full wave vector fields, mobile charge densities, as well as mobile charge and crystal lattice temperatures. Linear and nonlinear lossy transmission lines are used to demonstrate the simulator.

1. INTRODUCTION

Decades of research in computational electromagnetics and electronics have led to both sophisticated full wave field solvers and advanced semiconductor device simulators. However, both types of computation typically incorporate certain simplifying assumptions that limit their applications. For example, full wave field solvers commonly approximate charge transport as a linear process in which the mobile charge flux is directly proportional to the electric field. On the other hand, while active semiconductor device simulators offer a much more detailed description of nonlinear charge dynamics, they typically treat the fields with the electrostatic approximation. Although there are many important applications for these two distinctly different treatments of the electromagnetic interaction, current technological trends have created a need to unify the two approaches.

Advances in high performance microelectronics have produced smaller component sizes, higher circuit densities, and increased operating frequencies. These advances have led to full wave phenomena that affect the behavior of active components and circuits. For example, at clock speeds above a few hundred megahertz, surface waves, propagation delays, as well as unintended radiation, causing crosstalk between densely integrated components, can become important. At still higher frequencies, e.g. in the millimeter wave range, there may even be a qualitative shift in the way individual active components behave. As fields fluctuate at rates comparable to mobile charge momentum and energy relaxation rates, an active device can behave less as a nonlinearly component that manipulates a signal and more like a linear passive element that stores electromagnetic energy.

Aside from unintended consequences, other advanced technologies exploit the tight nonlinear coupling between electromagnetic radiation and mobile charges. For example, a possible ultrahigh frequency modulation scheme for laser diodes is based on heating degenerate two-dimensional gases of mobile charges in a quantum well with terahertz radiation (Li and Ning 2000). Another new technology uses hot electron induced real space transfer in the channel of a short gate length HEMT to emit terahertz radiation, providing a useful compact source for radiation in this frequency range (Knap et al. 2004). Simulating nonlinear charge transport with full wave electromagnetics is required to advance these new technologies as well as to understand the full wave parasitics in high speed microelectronics.

The need for full wave treatment of active devices has led to work on combining full wave field solvers and semiconductor device simulators. While virtually all these efforts treat the fields using the Finite Difference Time Domain (FDTD) method developed by Yee (Yee 1966), they differ in the levels of detail with which they treat active devices. Some approaches replace the active devices with lumped parameter equivalent circuits which impose field controlled current sources on certain edges of the FDTD mesh (Sui et al. 1992), (Piket-May et al. 1994), (Ciampolini et al. 1996). Other approaches treat carrier transport directly by coupling the FDTD field equations to the Boltzmann equation, solved classically with drift-diffusion or hydrodynamic theory (Sano and Shibata 1990), (Alsunaidi et al. 1996), (Mavahhedi and Abdipour 2006) or semi-classically with the Monte Carlo method (El-Ghazaly et al. 1990), (Goodnick et al. 1995).

Although different full wave simulations of active devices treat charge transport differently, their common use of FDTD field discretization gives them certain similarities. For example, FDTD requires a structured mesh and uses explicit time stepping. Explicit time stepping can be performed without factoring a large Jacobian matrix to determine the rotational fields. On the surface, this is a great advantage, allowing the solution of problems with tens of millions of unknowns (Piket-May et al. 1994). However, this advantage is undone, at least in part, by the highly nonlinear coupling of the fields and the mobile charge fluxes. This tight coupling imposes severe discretization restrictions that can require dense meshes, refined in terms of the Debye length, to represent the Boltzmann equation (Alsunaidi et al. 1996), (Mavahhedi and Abdipour 2006) and very short time steps determined by the Courant condition. With these discretization requirements, solving a relatively

Report Documentation Page

Form Approved
OMB No. 0704-0188

Public reporting burden for the collection of information is estimated to average 1 hour per response, including the time for reviewing instructions, searching existing data sources, gathering and maintaining the data needed, and completing and reviewing the collection of information. Send comments regarding this burden estimate or any other aspect of this collection of information, including suggestions for reducing this burden, to Washington Headquarters Services, Directorate for Information Operations and Reports, 1215 Jefferson Davis Highway, Suite 1204, Arlington VA 22202-4302. Respondents should be aware that notwithstanding any other provision of law, no person shall be subject to a penalty for failing to comply with a collection of information if it does not display a currently valid OMB control number.

1. REPORT DATE	2. REPORT TYPE	3. DATES COVERED
01 NOV 2006	**N/A**	**-**

4. TITLE AND SUBTITLE	5a. CONTRACT NUMBER
Classical Model Of The Electromagnetic Interaction Suitable For High Speed Semiconductor Device Simulation	5b. GRANT NUMBER
	5c. PROGRAM ELEMENT NUMBER
6. AUTHOR(S)	5d. PROJECT NUMBER
	5e. TASK NUMBER
	5f. WORK UNIT NUMBER
7. PERFORMING ORGANIZATION NAME(S) AND ADDRESS(ES) **US Army Research Lab Aberdeen Proving Ground, MD 21005**	8. PERFORMING ORGANIZATION REPORT NUMBER
9. SPONSORING/MONITORING AGENCY NAME(S) AND ADDRESS(ES)	10. SPONSOR/MONITOR'S ACRONYM(S)
	11. SPONSOR/MONITOR'S REPORT NUMBER(S)

12. DISTRIBUTION/AVAILABILITY STATEMENT
Approved for public release, distribution unlimited

13. SUPPLEMENTARY NOTES
See also ADM002075., The original document contains color images.

14. ABSTRACT

15. SUBJECT TERMS

16. SECURITY CLASSIFICATION OF:			17. LIMITATION OF ABSTRACT	18. NUMBER OF PAGES	19a. NAME OF RESPONSIBLE PERSON
a. REPORT	b. ABSTRACT	c. THIS PAGE			
unclassified	**unclassified**	**unclassified**	**UU**	**8**	

Standard Form 298 (Rev. 8-98)
Prescribed by ANSI Std Z39-18

small problem domain can require millions of solution variables solved repeatedly for tens of thousands of time steps. Finally, the "leapfrog" scheme FDTD uses to step through time means that at no moment during the simulation are the electric and magnetic fields and the mobile charge fluxes self-consistent. In addition to adding to stability problems, lack of self-consistency means that the highly nonlinear exchange of energy between the electromagnetic fields and the mobile charges is never fully represented.

This paper presents a self-consistent classical model of the electromagnetic interaction suitable for full wave simulation of active semiconductor devices. Electromagnetic fields are discretized using a new scheme called Delaunay/Voronoi Surface Integration (DVSI) which allows unstructured tetrahedral meshes. The mobile charge and energy fluxes are derived from moments of the Boltzmann equation and incorporate a new treatment of heat flow derived from the heat capacity of Fermi gases. The field equations are solved self-consistently with the charge and energy transport equations. This greatly improves the stability of the simulator so that discretization is determined solely by variations in the solution variables. That is, the mesh need only be refined enough to adequately represent field wavelengths and rapid changes in charge densities, e.g. dopant junctions, heterojunctions, Schottky barriers. Likewise, time steps need only by small enough to represent dynamic variations in the solution variables. This permits adaptive time stepping where time steps may vary by several orders of magnitude during the course of a simulation. To demonstrate the model, certain linear and nonlinear lossy transmission line simulations are presented.

2. FULL WAVE NONLINEAR CHARGE TRANSPORT

Maxwell's vector field theory and his kinetic theory of gases form a complete and self-consistent model of the electromagnetic interaction. The model consists of Maxwell's static and dynamic field equations as well as the equations for charge and energy conservation. Charge and energy conservation can be derived from moments of the Boltzmann equation, and the fluxes that appear in these conservation laws can also be obtained from moments of the Boltzmann equation with special attention payed to the thermodynamics of ideal gases.

2.1 Maxwell's Field Equations

The behavior of electromagnetic fields is completely determined by Maxwell's equations.

$$\nabla \cdot \epsilon \boldsymbol{E} = \rho \tag{1}$$

$$\nabla \cdot \mu \boldsymbol{H} = 0 \tag{2}$$

$$\nabla \times \boldsymbol{H} = \boldsymbol{J} + \frac{\partial \epsilon \boldsymbol{E}}{\partial t} \tag{3}$$

$$\nabla \times \boldsymbol{E} = -\frac{\partial \mu \boldsymbol{H}}{\partial t} \tag{4}$$

where (1) and (2) are Gauss's electrostatic and magnetostatic laws respectively, (3) is Ampere's law, (4) is Faraday's law, ϵ is the dielectric constant, μ is the magnetic permeability, $\boldsymbol{E}$ is the electric field, $\boldsymbol{H}$ is the magnetic field, ρ is the charge density, and $\boldsymbol{J}$ is the mobile charge flux. The charge density is determined locally by the concentration of mobile electrons n, mobile holes p, ionized donor impurities N_D^+, and ionized acceptors N_A^-. The charge flux is determined locally by mobile electron and hole fluxes. The charge densities and fluxes are obtained from the transport model.

To find the electric and magnetic fields that satisfy the four Maxwell's equations, the electric field can be expressed in terms of vector and scalar potentials, $\boldsymbol{A}$ and ψ respectively.

$$\boldsymbol{E} = -\left(\frac{\partial \boldsymbol{A}}{\partial t} + \nabla\psi\right) = \boldsymbol{E}_{\text{rot}} + \boldsymbol{E}_{\text{irr}} \tag{5}$$

Since the curl of a gradient is always zero, $\nabla\psi$ represents a conservative, irrotational electric field. To make the two electric field components functionally orthogonal, a zero divergence is assigned to the divergence of the vector potential's displacement.

$$\nabla \cdot \epsilon \frac{\partial \boldsymbol{A}}{\partial t} = 0$$

This is equivalent to the Coulomb gauge for a homogeneous medium. It allows the time derivative of the vector potential to be viewed as an entirely rotational electric field.

From Faraday's law, the magnetic flux density is given by the curl of the vector potential.

$$\mu \boldsymbol{H} = \nabla \times \boldsymbol{A}$$

Since the divergence of a curl is always zero, Gauss's magnetostatic law is automatically satisfied. This means that the magnetic field is treated as entirely rotational, which is valid for homogeneous permeability. For nonhomogeneous μ, e.g. ferrites, the magnetic field should be expressed in terms of rotational and conservative components, similar to (5). However, this paper only considers homogeneous permeability.

2.2 Classical Charge Transport

For classical systems, charges can be treated as particles with their behavior determined by the Boltzmann equation. A relatively efficient way to solve this equation treats the charges as ideal Fermi gases. An ideal Fermi gas in three dimensions is spherically symmetric in momentum space, and its distribution in energy is determined by its chemical potential and temperature according to Fermi-Dirac statistics.

$$f_n = \frac{1}{\exp\left(\frac{E - F_n}{kT_n}\right) + 1}$$

where f_n is the occupation probability of an electron in the conduction band of a semiconductor, E is the electron energy, F_n is its chemical potential (quasi-Fermi level), and T_n is the electron temperature. An analogous expression exists for the distribution function of positively charged holes in the valence band. The effective mass approximation for band structure can be used to integrate f_n over all available

momentum states and define the local electron density.

$$\begin{aligned} n &= \frac{\sqrt{2}m_n^{3/2}}{\pi^2\hbar^3}\int_{E_C}^{\infty}\frac{\sqrt{E-E_C}}{\exp\left(\frac{E-F_n}{kT_n}\right)+1}dE \\ &= N_C(kT)^{3/2}F_{1/2}(\eta_n) \end{aligned}$$

where m_n is the effective mass for electrons, E_C is the conduction band edge, F_i is the Fermi integral of degree i, and $\eta_n = (F_n - E_C)/(kT_n)$. A similar expression exists for the density of holes in the valence band. Fermi-Dirac statistics is also used to calculate the density of ionized dopant impurities. The electron energy density is obtained in a similar manner.

$$E_n = N_C(kT)^{5/2}F_{3/2}(\eta_n)$$

The classical charge transport model is obtained from moments of the Boltzmann equation, expressed in terms of the relaxation time and effective mass approximations (Hess 2000). For electrons, the moments have the following form.

$$\frac{1}{4\pi^3}\int\mathcal{O}\left\{f_n+\tau\frac{\partial f_n}{\partial t}=\frac{\tau}{\hbar}\boldsymbol{F}\cdot\nabla_{\mathrm{k}}f_n-\tau\boldsymbol{v}\cdot\nabla f_n\right\}d\boldsymbol{k} \quad (6)$$

where τ is the momentum relaxation time, $\boldsymbol{v}$ is the electron velocity, and $\boldsymbol{k}$ is its momentum vector. The total force $\boldsymbol{F}$ acting on the electron includes both the Coulomb and Lorentz forces.

$$\boldsymbol{F} = -q(\boldsymbol{E}+\boldsymbol{v}\times\boldsymbol{B})$$

Different moments are obtained with different choices of the operator $\mathcal{O}$ acting on the Boltzmann equation.

Electron conservation is obtained by setting $\mathcal{O}=1$ and integrating over all $\boldsymbol{k}$-states to obtain the zeroth moment.

$$-\frac{\partial n}{\partial t} = \nabla\cdot\boldsymbol{J}_n + U_n$$

where $\boldsymbol{J}_n$ is the electron flux and U_n is the net recombination rate. This paper considers only the Shockley-Hall-Read recombination mechanism (Hess 2000). The electron flux $\boldsymbol{J}_n$ is obtained by setting $\mathcal{O}=\boldsymbol{v}$ and integrating over all $\boldsymbol{k}$ states to yield the drift-diffusion flux.

$$\begin{aligned} \boldsymbol{J}_n+\bar{\tau}\frac{\partial\boldsymbol{J}_n}{\partial t} &= -\mu_n N_C\frac{\bar{\boldsymbol{M}}}{1+\mu_n^2\boldsymbol{B}^2}\times \\ &\Big[(kT)^{3/2}F_{1/2}\boldsymbol{E}+ \\ &(kT)^{3/2}F_{1/2}\nabla\left(\frac{2}{3}\frac{F_{3/2}}{F_{1/2}}\frac{kT}{q}\right)+ \\ &\left(\frac{2}{3}\frac{F_{3/2}}{F_{1/2}}\frac{kT}{q}\right)\nabla(kT)^{3/2}F_{1/2}\Big] \end{aligned} \quad (7)$$

where $\bar{\tau}$ is an average momentum relaxation lifetime, μ_n is the electron mobility, $\boldsymbol{B}=\mu\boldsymbol{H}$ is the magnetic flux density, and $\bar{\boldsymbol{M}}$ is a tensor that generates the vortex flux components produced by the Lorentz force.

$$\bar{\boldsymbol{M}} = \begin{bmatrix} M_{xx} & M_{xy} & M_{xz} \\ M_{yx} & M_{yy} & M_{yz} \\ M_{zx} & M_{zy} & M_{zz} \end{bmatrix}$$

$$\begin{aligned} M_{xx} &= 1+\mu_n^2B_x^2 \\ M_{xy} &= -\mu_nB_z+\mu_n^2B_xB_y \\ M_{xz} &= \mu_nB_y+\mu_n^2B_xB_x \\ M_{yx} &= \mu_nB_z+\mu_n^2B_xB_y \\ M_{yy} &= 1+\mu_n^2B_y^2 \\ M_{yz} &= -\mu_nB_x+\mu_n^2B_yB_z \\ M_{zx} &= -\mu_nB_y+\mu_n^2B_xB_z \\ M_{zy} &= \mu_nB_x+\mu_n^2B_yB_z \\ M_{zz} &= 1+\mu_n^2B_z^2 \end{aligned}$$

The drift-diffusion flux (7) is discretized using the Scharfetter-Gummel method (Scharfetter and Gummel 1969). The resulting net flux along a mesh edge of length L connecting vertices 1 and 2 is given by the following.

$$\begin{aligned} J_{n,\mathrm{net}}^{1\to2}+\bar{\tau}\frac{\partial J_{n,\mathrm{net}}^{1\to2}}{\partial t} &= \left(\frac{2}{3}\frac{F_{3/2}}{F_{1/2}}\frac{kT}{q}\right)_{\mathrm{ave}}\times \\ &\frac{\mu_n\bar{\boldsymbol{M}}}{1+\mu_n^2\boldsymbol{B}^2}\frac{N_C}{L}\times \\ &\Big[B(\xi_n)(kT_{n,1})^{3/2}F_{1/2}(\eta_{n,1})- \\ &B(-\xi_n)(kT_{n,2})^{3/2}F_{1/2}(\eta_{n,2})\Big] \\ &= J_n^{1\to2}-J_n^{2\to1} \end{aligned} \quad (8)$$

$$B(\xi_n) = \frac{\xi_n}{\exp(\xi_n)-1}$$

$$\xi_n = L\left(\frac{3}{2}\frac{F_{1/2}}{F_{3/2}}\frac{q}{kT_n}\right)_{\mathrm{ave}}\left[E_{1\to2}+\frac{1}{L}\Delta\left(\frac{2}{3}\frac{F_{3/2}}{F_{1/2}}\frac{kT_n}{q}\right)\right]$$

Conservation of electron energy can also be derived from (6). The energy continuity equation is obtained by setting $\mathcal{O}=E$ and integrating over all $\boldsymbol{k}$-states to obtain the second moment.

$$-\frac{\partial E_n}{\partial t} = q\boldsymbol{E}\cdot\boldsymbol{J}_n+\nabla\cdot\boldsymbol{S}_n^{\mathrm{tot}}+U_E$$

where $\boldsymbol{S}_n^{\mathrm{tot}}$ is the total electron energy flux and U_E is the net loss of energy to both recombination and phonon scattering.

$$U_E = \langle E_n^{\mathrm{kin}}\rangle U_n + n\frac{F_{3/2}}{F_{1/2}}\left(\frac{kT_n-kT_{\mathrm{lat}}}{\tau_n}\right)$$

where $\langle E_n^{\mathrm{kin}}\rangle$ is the average kinetic energy, T_{lat} is the temperature of the semiconductor crystal, and τ_n is the energy relaxation lifetime.

The components of total energy flux are known from the thermodynamics of ideal Fermi gases. In drift-diffusion, when a charge moves through space, it is removed from one Fermi gas with a particular chemical potential and temperature, and it is transferred to another Fermi gas with a different chemical potential and temperature. Obviously, the internal (kinetic) energy of the transferred charges is part of the total energy exchanged between the gases. If the gases have different chemical potentials with respect to their ground states, then there is also a certain amount of

chemical work that also counts as an energy transfer. Finally, if the gases have different temperatures, then transferred charges must be heated or cooled to the temperature of the receiving gas. This thermalization process has the form of heat flow between the two Fermi gases.

Setting $\mathcal{O} = \boldsymbol{v}E$ in (6) and integrating over all $\boldsymbol{k}$-states is the third moment and accounts for both the internal energy and chemical work components of the total flux. Applying the Scharfetter-Gummel method then results in the following discrete expression for these components of energy flux between neighboring gases 1 and 2.

$$\begin{aligned} S^{1\to2}_{kw,\text{net}} + \bar{\tau}\frac{\partial S^{1\to2}_{kw,\text{net}}}{\partial t} &= \left(\frac{2}{5}\frac{F_{5/2}}{F_{3/2}}\frac{kT}{q}\right)_{\text{ave}} \times \\ &\quad \frac{\mu_n \bar{\boldsymbol{M}}}{1+\mu_n^2\boldsymbol{B}^2}\frac{N_C}{L} \times \\ &\quad \Big[B(\xi_E)(kT_{n,1})^{5/2}F_{3/2}(\eta_{n,1}) - \\ &\quad B(-\xi_E)(kT_{n,2})^{5/2}F_{3/2}(\eta_{n,2})\Big] \\ &= S^{1\to2}_{kw} - S^{2\to1}_{kw} \end{aligned} \tag{9}$$

$$\xi_E = L\left(\frac{3}{2}\frac{F_{3/2}}{F_{5/2}}\frac{q}{kT_n}\right)_{\text{ave}}\left[\frac{5}{3}E_{1\to2} + \frac{1}{L}\Delta\left(\frac{2}{3}\frac{F_{5/2}}{F_{3/2}}\frac{kT_n}{q}\right)\right]$$

Transport simulators based on both drift-diffusion and hydrodynamics treat heat flow between gases according to the Stratton model (Stratton 1962), which expresses it in terms of a thermal conductivity of the charges and a temperature gradient. However, the heat required to thermalize charges moving from one gas to another can be more precisely defined in terms of the heat capacity of Fermi gases.

$$C_V \equiv (E - F_n)\frac{d}{d(kT_n)}$$

The net heat flow can then be obtained by defining the operator in (6) as $\mathcal{O} = \boldsymbol{v}C_V$, evaluating the temperature derivatives of the distribution function f_n, integrating over all $\boldsymbol{k}$-states, applying the Scharfetter-Gummel discretization scheme, and integrating the exchanged charges from their initial to final temperatures. The resulting discretized net heat flow is then given by the following.

$$\begin{aligned} S^{1\to2}_{\text{heat,net}} + \bar{\tau}\frac{\partial S^{1\to2}_{\text{heat,net}}}{\partial t} &= [S^{1\to2}_{kw} - S^{1\to2}_{kw,T_{n,2}} - \\ &\quad F_{n,1}(J^{1\to2}_n - J^{1\to2}_{n,T_{n2}})] - \\ &\quad [S^{2\to1}_{kw} - S^{2\to1}_{kw,T_{n,1}} - \\ &\quad F_{n,2}(J^{2\to1}_n - J^{2\to1}_{n,T_{n1}})] \end{aligned}$$

where $S^{i\to j}_{kw}$ are the same energy fluxes defined in (9) and $S^{i\to j}_{kw,T_{n,j}}$ are those same fluxes calculated with both gases held at $T_{n,j}$. Likewise, $J^{i\to j}_n$ are the same charge fluxes defined in (8) and $J^{i\to j}_{n,T_{n,j}}$ are those same fluxes with both gases at $T_{n,j}$. Analogous discrete expressions exist for the net mobile hole charge and energy fluxes, $\boldsymbol{J}_p$ and $\boldsymbol{S}^{\text{tot}}_p$ respectively.

2.3 Lattice Heating

The vector field equations in Section 2.1 along with the charge and energy fluxes in Section 2.2 form a physically self-consistent classical model of the electromagnetic interaction. When solved simultaneously, they show how dynamic fields and mobile charges interact within an idealized semiconductor that acts as a perfect heat sink always remaining at room temperature. However, real semiconductors have finite thermal conductivities and heat capacities that result in lattice heating as current passes through them. To account for this, an additional equation balancing the production of lattice energy by Joule's heat with its dissipation by thermal diffusion is also solved.

$$-\rho_s C_p \frac{\partial T_{\text{lat}}}{\partial t} = \nabla\cdot\kappa\nabla T_{\text{lat}} - \boldsymbol{E}_{\text{applied}}\cdot q(\boldsymbol{J}_p - \boldsymbol{J}_n)$$

where ρ_s is the semiconductor's density, C_p is its specific heat, and κ is its thermal conductivity.

2.4 Time Stepping

For general input excitations, including sharp large signal pulses, mobile charge densities and temperatures can initially fluctuate very rapidly (femtosecond time scales). Later these fluctuations dampen as the system approaches a new steady state. The damping process can take a relatively long time, reaching steady state after tens or hundreds of nanoseconds. Spanning this wide dynamic range requires adaptive time stepping.

All dynamic quantities in this model are treated as piece-wise linear in time, and their time derivatives are evaluated with the fully implicit backward Euler method. Therefore, any solution variable ϕ at time step i is approximated by the first two terms of a generally infinite series.

$$\phi_i = \phi_{i-1} + \dot{\phi}_{i-1}\Delta t + \frac{1}{2}\ddot{\phi}_{i-1}\Delta t^2 + \cdots$$

The third term in the series serves as a measure of ϕ's deviation from linearity and as a useful criterion for determining the next time step. When ϕ_i is computed, simple estimates of its time derivatives are calculated.

$$\dot{\phi}_i \approx \frac{\phi_i - \phi_{i-1}}{\Delta t_i}; \qquad \dot{\phi}_{i-1} \approx \frac{\phi_{i-1} - \phi_{i-2}}{\Delta t_{i-1}}$$

$$\ddot{\phi}_{i-1} \approx \frac{\dot{\phi}_i - \dot{\phi}_{i-1}}{(\Delta t_i + \Delta t_{i-1})/2}$$

After a maximum relative error $\epsilon_{\max}$ is chosen, the second derivative can then be used to determine the next appropriate time step.

$$\Delta t_{i+1} = \sqrt{2\epsilon_{\max}\phi_i/\ddot{\phi}_{i-1}}$$

Using $\epsilon_{\max} = 0.001$, following this procedure for the electron and hole chemical potentials and temperatures as well as for the lattice temperature, and using the smallest computed Δt_{i+1} as the next time step has been an effective way to capture the wide dynamic range that electron devices can exhibit.

3. DELAUNAY/VORONOI SURFACE INTEGRATION

To express the equations in Section 2 so that they can be solved simultaneously, the useful properties of a Delaunay mesh (Delaunay 1934) representing the problem domain can be employed. A contiguous set of tetrahedrons satisfies the Delaunay criterion if none of the vertices lie within any of the tetrahedrons' circumspheres. When this is true, a reciprocal mesh, whose vertices are the circumcenters of the tetrahedrons, can be computed. The reciprocal mesh is the dual of the primary Delaunay mesh, and it consists of contiguous Voronoi polyhedrons that fill the problem domain. Figure 1 shows a set of Delaunay tetrahedrons that share a common primary edge and the Voronoi polygon that corresponds to that edge. The edge is, by definition, perpendicular to the polygon.

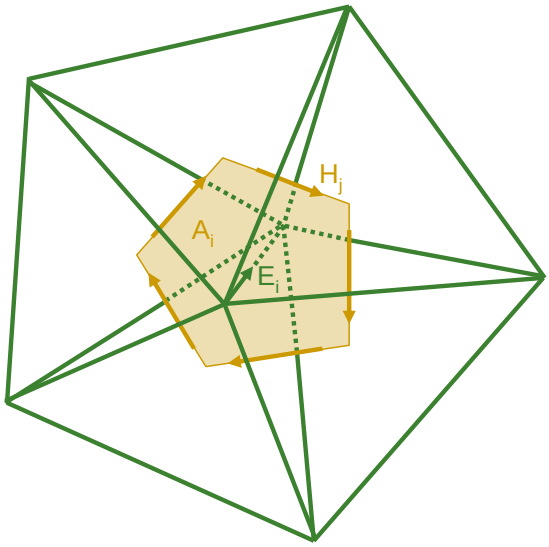

Fig. 1: Delaunay tetrahedrons sharing a common edge and the Voronoi polygon facet formed by their circumcenters.

The relationship between the primary edge and the dual polygon provides an easy way to represent Ampere's law. A projection of an electric field is assigned to each primary edge, and projections of magnetic fields are assigned to the dual edges that form the perimeter of the Voronoi polygon. The value of the electric field E_i on a primary edge is defined by integrating (3) over the area of the polygon A_i and applying the Stokes curl theorem.

$$\int_{A_i} \left(\boldsymbol{J} + \frac{\partial \epsilon \boldsymbol{E}}{\partial t} \right) \cdot d\boldsymbol{a} = \int_{A_i} \nabla \times \boldsymbol{H} \cdot d\boldsymbol{a} = \oint_{\partial A_i} \boldsymbol{H} \cdot d\boldsymbol{l}$$

$$\left(J_i + \frac{\partial \epsilon E_i}{\partial t} \right) A_i = \sum_j H_j L_j \qquad (10)$$

In this way, the electric field projection on each primary edge is defined in terms of magnetic field projections on dual edges.

The relationship between Delaunay meshes and their Voronoi reciprocals also offers a convenient way to define the magnetic field projections assigned to dual edges. Figure 2 shows that every dual edge is perpendicular to a primary triangle. The projection of the magnetic field H_j on

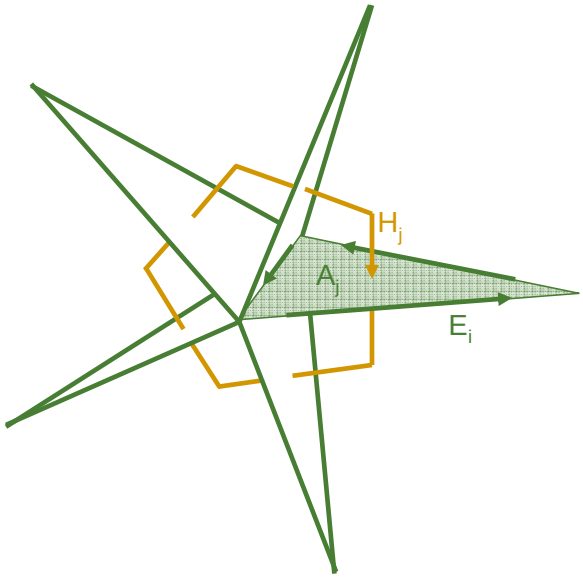

Fig. 2: Dual edges are perpendicular to primary Delaunay triangles.

a dual edge is defined by integrating (4) over the area of its corresponding primary triangle A_j and applying the Stokes curl theorem.

$$-\int_{A_j} \frac{\partial \mu \boldsymbol{H}}{\partial t} \cdot d\boldsymbol{a} = \int_{A_j} \nabla \times \boldsymbol{E} \cdot d\boldsymbol{a} = \oint_{\partial A_j} \boldsymbol{E} \cdot d\boldsymbol{l}$$

$$-\frac{\partial \mu H_j}{\partial t} A_j = \sum_i E_i L_i \qquad (11)$$

Applying this procedure to each dual edge and combining the results with the equations for the electric field projections (10) produces a set of linearly independent equations that can be solved to determine the electric and magnetic fields throughout the problem domain.

In addition to providing convenient ways to represent the curl operators in Ampere's and Faraday's laws, the Delaunay and Vornoi meshes can be used to represent the divergence operators that appear in electrostatics as well as charge and energy conservation. Referring back to Figure 1, each primary edge can be associated with a Voronoi polygon. As shown in Figure 3, each primary vertex belongs to a number of primary edges, all of which have Voronoi polygons that fit together contiguously to form a polyhedron enclosing the vertex. To evaluate the divergence of a flux, such as the electric displacement in Gauss's electrostatic law, it is first integrated over the volume of the polyhedron. By the divergence theorem, the volume integral of the divergence is equivalent to the integral of the flux over the surface area of the polyhedron. This surface integral is evaluated by simply visiting each primary edge to which the vertex belongs, evaluating the flux on the edge, and multiplying it

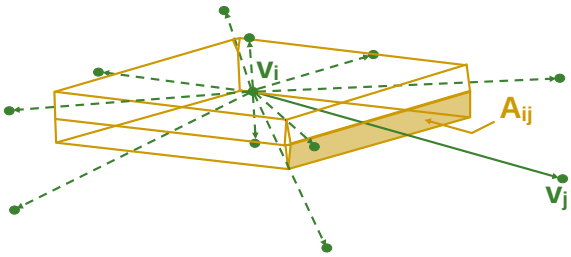

Fig. 3: The Voronoi polygons for all the primary edges containing a particular vertex form a faceted polyhedron that encloses the vertex. This polyhedron is used in the box integration method to represent divergences away from the vertex.

by the area of its associated dual polygon.

$$\int_{V_i} \nabla \cdot \epsilon \boldsymbol{E} dv = \oint_{\partial V_i} \epsilon \boldsymbol{E} \cdot d\boldsymbol{a} = \sum_j \epsilon \frac{\psi_i - \psi_j}{L_{ij}} A_{ij}$$

The procedure is called the box integration method and is widely used in semiconductor device simulation.

To summarize, DVSI is used to represent Ampere's and Faraday's laws on the Delaunay mesh, and box integration is used to represent Gauss's electrostatic law, the continuity of electrons and holes, the conservation of electron and hole energies, as well as the conservation of lattice energy. The result is a set of highly nonlinear coupled differential equations which is solved simultaneously with the full Newton method. The solutions show the full wave behavior of the electromagnetic fields coupled to the nonlinear thermodynamics of the mobile charges at each moment of time considered during the simulation.

4. RESULTS AND DISCUSSION

To test the simulation, the simple lossy transmission line shown in Figure 4 is considered. It consists of two

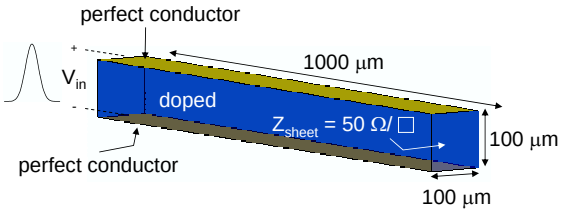

Fig. 4: A parallel conductor transmission line with a doped semiconductor serving as a lossy substrate and a 50 Ω termination at the output.

ideal metal contacts on a doped semiconductor substrate terminated with a 50 Ω impedance. For the first test case, the metals form ohmic contacts with the substrate, which is treated as uniformly doped (10^{15} cm^{-3} p-type) silicon. The line is excited with Gaussian time domain input signals, and the S_{21} scattering parameters are extracted from Fourier analyses of the simulated input and output voltages and currents. This simple, highly linear test case permits accurate analytic approximations for the S-parameters derived from the telegraphist's equations (Ramo et al. 1984). Comparing the analytic S-parameters with the simulated values is a useful test of both the charge transport model and the field solutions.

Figure 5 compares the derived S-parameters with their simulated values, computed with both full wave electromagnetics and with the quasi-static approximation. The full

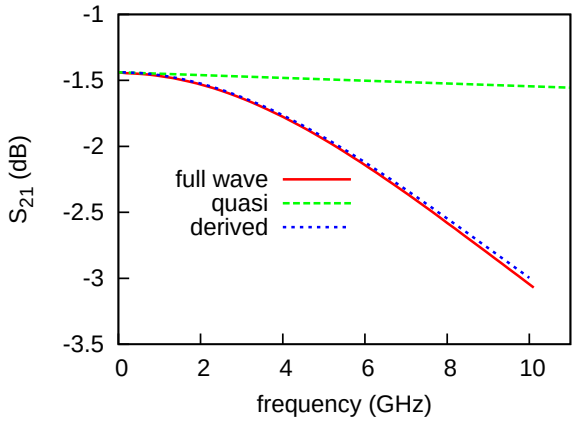

Fig. 5: Simulated S-parameters for the lossy transmission line in Figure 4 compared to those derived from the telegraphist's equations. The metals form ohmic contacts with the p-type silicon substrate. The simulated data labeled "full wave" were computed with full wave electromagnetics, and those labeled "quasi" used the quasi-static field approximation.

wave data compare favorably with the analytic solutions, with the increasing error at higher frequencies most likely due to decreasing Fourier components of the input signal. A flatter input spectrum decreases the error. Figure 4 also shows very poor agreement between the quasi-static and analytic solutions. This is interesting because full wave effects are typically thought of in terms of interference that occurs when feature sizes are comparable to wavelength. When feature sizes are much smaller than the wavelength, the quasi-static field approximation is typically considered appropriate. However, the transmission line in Figure 4 is an order of magnitude shorter than the smallest signal wavelength considered, and yet the quasi-static approximation is highly inaccurate.

The electrically short transmission line exhibits the significant full wave effect shown in Figure 5 because quasi-static fields do not store energy. When the Gaussian input signal is applied, energy is injected into the line, and that energy will persist for as long as it takes the terminating impedance and the mobile charges in the substrate to dissipate it. The energy is stored in the form of rotational

electric and magnetic fields, determined by Ampere's and Faraday's laws. Since the quasi-static approximation does

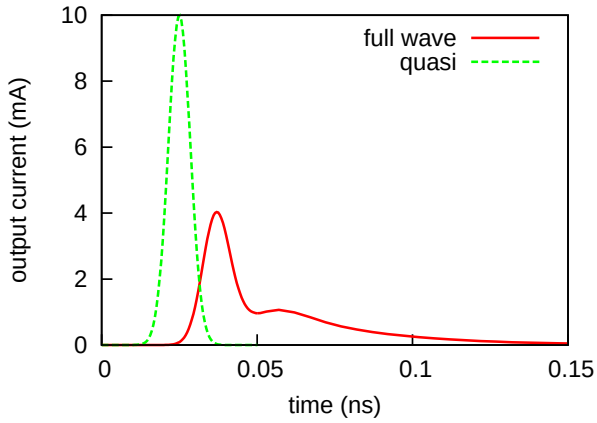

Fig. 6: Simulated output currents for the lossy transmission line in Figure 4 excited by a Gaussian input voltage signal. The currents labeled "full wave" were computed with full wave electromagnetics, and those labeled "quasi" used the quasi-static field approximation.

not consider these fields, the current delivered to the output impedance simply follows the input voltage and is unable to represent the currents that persist after the input signal goes to zero, as shown in Figure 6.

A nonlinear example, in which the top metal in Figure 4 forms a Schottky contact with a doped (10^{15} cm^{-3} n-type) GaAs substrate, was also considered. The rectifying Schottky contact blocks current for negative applied voltages but allows the substrate to conduct significant currents under sufficiently large positive voltages. It also produces a very narrow depletion region beneath the top metal that greatly increases the transmission line's capacitance. Figure 7 shows S-parameter computed around quiescent bias points of 0 V (nonconducting) and 2 V (highly conducting). The nonlinear properties of this transmission line make its frequency characteristics strong functions of its bias condition, and like the previous example, high frequency solutions require full wave electromagnetics.

4. CONCLUSIONS

Maxwell's field equations and the thermodynamics of ideal Fermi gases of charged particles form a complete and physically self-consistent classical model of the electromagnetic interaction. The remarkable compatibility of the vector calculus of the fields and the statistical mechanics of the charges is not coincidental. Since Maxwell developed the field theory while he was also working on the kinetic theory of gases, it is likely the two theories were intended to work together. Although the quantum mechanics of fermions required the Maxwell-Boltzmann distribution of the charged particles to be replaced with the more general Fermi-Dirac distribution, the essential physics is the same. The field theory has not required any modification from its original form.

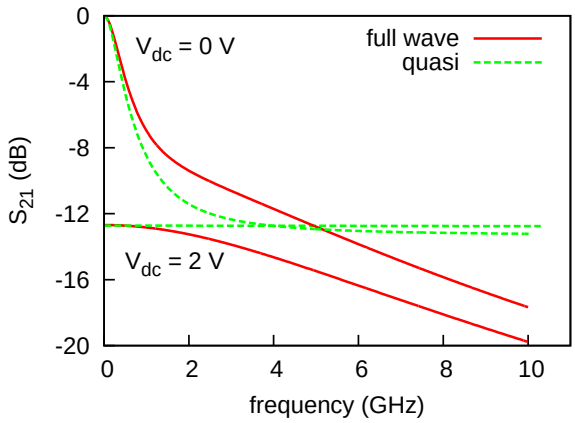

Fig. 7: Simulated S-parameters for the lossy transmission line in Figure 4 with the top metal forming a Schottky contact with an n-type GaAs substrate. The voltage labels show the quiescent biases. Curves labeled "full wave" were computed with full wave electromagnetics, and those labeled "quasi" used the quasi-static field approximation.

Although the necessary pieces of a complete classical theory of the electromagnetic interaction have been in place for a long time, the model had not been computed self-consistently. The most commonly developed techniques for treating the vector field components of the model have not been well suited for highly nonlinear charge transport, and the techniques developed for nonlinear charge transport have not been generalized to treat vector fields self-consistently. This paper has presented a new discretization scheme called DVSI that overcomes these obstacles by representing both the curls of vector fields and the divergences of fluxes in a self-consistent manner.

DVSI permits the fully coupled solution of the classical electromagnetic interaction for highly nonlinear systems from dc to arbitrarily high frequencies. It was used to simulate lossy transmission lines that exhibit different degrees of nonlinearity. A highly linear case showed the simulated results to agree well with analytic solutions. This simple result also demonstrated that full wave electromagnetics can be important even when devices features are much smaller than signal wavelengths. This is true when the device is able to store electromagnetic energy. The energy is stored in the form of rotational fields determined by Ampere's and Faraday's laws. Additional simulations of nonlinear transmission lines showed that the high frequency characteristics strongly depend on the dc quiescent bias condition. Further potential uses for the code include the full wave simulation of high speed microelectronics and optoelectronics, which will be the subjects of future work.

ACKNOWLEDGEMENTS

This work was supported by the Defense Department's High Performance Computing Modernization Program under the User Productivitiy Enhancement and Technology Transfer contract #GS04T01BFC0061.

REFERENCES

Alsunaidi, M., S. Imtiaz, and S. El-Ghazaly, 1996: Electromagnetic wave effects on microwave transistors using a full-wave time-domain model. *IEEE Trans. Microwave Theory Tech.*, **44**, 799–808.

Ciampolini, P., P. Mezzanotte, L. Roselli, and R. Sorrentino, 1996: Accurate and efficient circuit simulation with lumped-element FDTD technique. *IEEE Trans. Microwave Theory Tech.*, **44**, 2207–2214.

Delaunay, B., 1934: Sur la sphère vide. *Bull. Acad. Sci. USSR(VII)*, 793–800.

El-Ghazaly, S., R. Joshi, and R. Grondin, 1990: Electromagnetic and transport considerations in subpicosecond photoconductive switch modeling. *IEEE Trans. Microwave Theory Tech.*, **38**, 629–637.

Goodnick, S., S. Pennathur, U. Ranawake, P. Lenders, and V. Tripathi, 1995: Parallel implementation of Monte Carlo particle simulation coupled to Maxwell's equations. *Int. Journal of Numerical Modelling: Electronic Networks, Devices and Fields*, **8(3-4)**, 205–219.

Hess, K., 2000: *Advanced Theory of Semiconductor Devices*. IEEE Press.

Knap, W., J. Lusakowski, T. Parenty, S. Bollaert, A. Cappy, V. Popov, and M. Shur, 2004: Terahertz emission by plasma waves in 60 nm gate high electron mobility transistors. *Appl. Phys. Lett.*, **84**, 2331–2333.

Li, J. and C. Ning, 2000: Plasma heating and ultrafast semiconductor laser modulation through a terahertz heating field. *J. Appl. Phys.*, **88**, 4933–4940.

Mavahhedi, M. and A. Abdipour, 2006: Efficient numerical method for simulation of high-frequency active devices. *IEEE Trans. Microwave Theory Tech.*, **54**, 2636–2645.

Piket-May, M., A. Taflove, and J. Baron, 1994: FD-TD modeling of digital signal propagation in 3-D circuits with passive and active loads. *IEEE Trans. Microwave Theory Tech.*, **42**, 1514–1523.

Ramo, S., J. Whinnery, and T. Van Duzer, 1984: *Fields and Waves in Communication Electronics, 2nd Ed.*. John Wiley & Sons.

Sano, E. and T. Shibata, 1990: Fullwave analysis of picosecond photoconductive switches. *IEEE J. Quantum Electron.*, **26**, 372–377.

Scharfetter, D. and D. Gummel, 1969: Large signal analysis of a silicon Read diode oscillator. *IEEE Trans. Electron Dev.*, **ED-16**, 64–77.

Stratton, R., 1962: Diffusion of hot and cold electrons in semiconductor barriers. *Phys. Rev.*, **126**, 2002–2014.

Sui, W., D. Christensen, and C. Durney, 1992: Extending the two-dimenional FD-TD method to hybrid electromagnetic systems with active and passive lumped elements. *IEEE Trans. Microwave Theory Tech.*, **40**, 724–730.

Yee, K., 1966: Numerical solution of initial boundary value problems involving Maxwell's equations in isotropic media. *IEEE Trans. Antennas Propagat.*, **14**, 302–307.